# *Supplementary Information*

*for*

# Effect of planetary boundary layer evolution on new particle formation events over Cyprus

Neha Deot[1], Vijay P. Kanawade[1,2*], Alkistis Papetta[1], Rima Baalbaki[3,1], Michael Pikridas[1], Franco Marenco[1], Markku Kulmala[3], Jean Sciare[1], Katrianne Lehtipalo[2,3], Tuija Jokinen[1*]

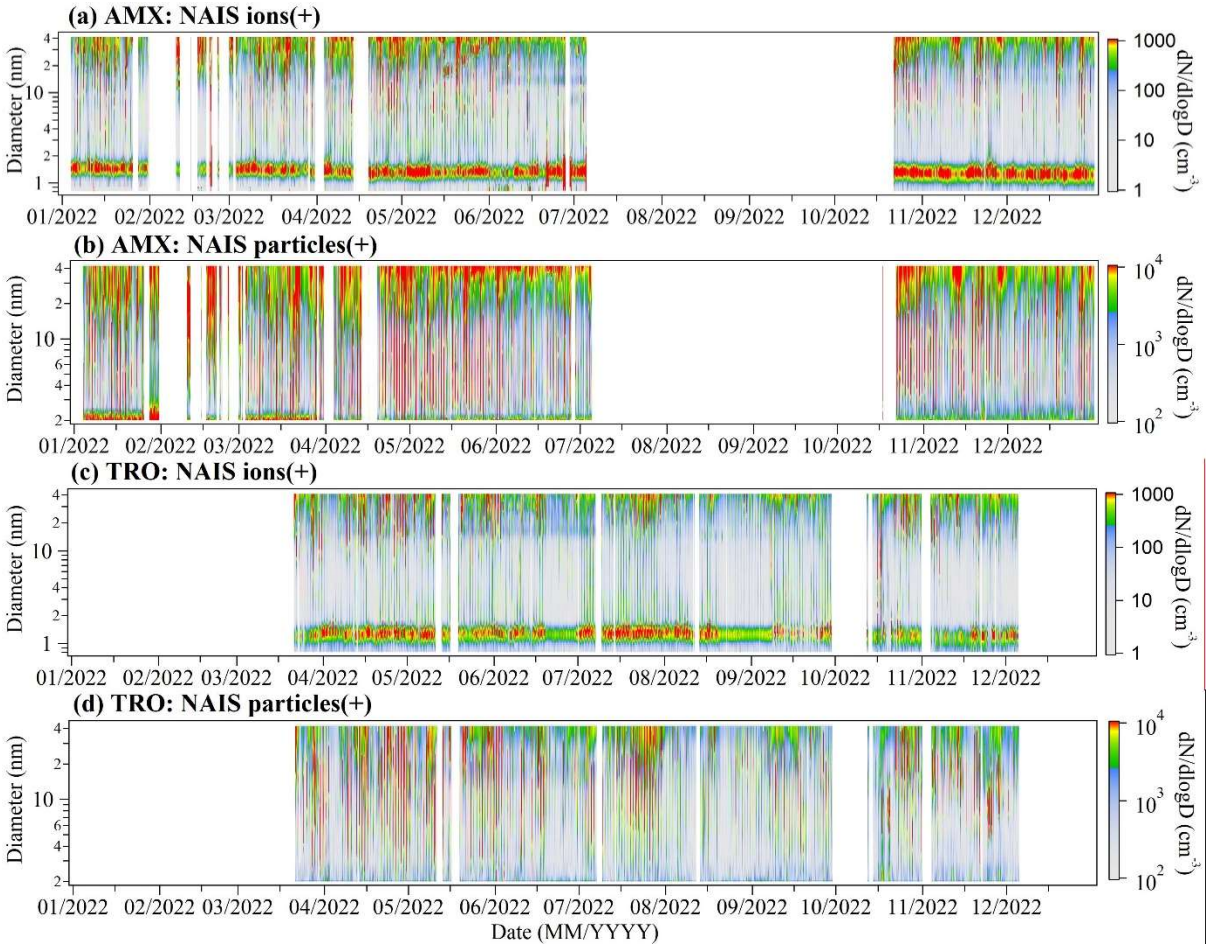


**Figure S1**. Time-evolution of positive polarity ion and particle number size distributions at AMX (a,b) and TRO (c,d) during the study period. The white spaces indicate data unavailability.

**Table S1.** The monthly number of NPF events, non-events, unclear days, and nodata days at AMX and TRO, and concurrent NPF events at both AMX and TRO sites.

| Month | AMX | | | | TRO | | | | Concurrent |
|---|---|---|---|---|---|---|---|---|---|
| | **NPF** | non-event | Unclear | nodata | **NPF** | non-event | Unclear | nodata | **NPF** |
| Jan | **12** | 6 | 6 | 7 | **0** | 0 | 0 | 31 | **0** |
| Feb | **0** | 0 | 3 | 25 | **0** | 0 | 0 | 28 | **0** |
| Mar | **15** | 3 | 10 | 3 | **4** | 0 | 5 | 22 | **3** |
| Apr | **23** | 1 | 2 | 4 | **22** | 7 | 1 | 0 | **19** |
| May | **23** | 4 | 4 | 0 | **20** | 2 | 3 | 6 | **17** |
| Jun | **11** | 11 | 6 | 2 | **11** | 11 | 8 | 0 | **7** |
| Jul | **3** | 1 | 0 | 27 | **22** | 2 | 2 | 5 | **2** |
| Aug | **0** | 0 | 0 | 31 | **5** | 10 | 14 | 2 | **0** |
| Sep | **0** | 0 | 0 | 30 | **16** | 1 | 12 | 1 | **0** |
| Oct | **10** | 0 | 0 | 21 | **10** | 1 | 5 | 15 | **10** |
| Nov | **18** | 5 | 6 | 1 | **9** | 3 | 14 | 4 | **9** |
| Dec | **14** | 12 | 5 | 0 | **2** | 2 | 0 | 27 | **2** |
| Total | **129** | 43 | 42 | 151 | **121** | 39 | 64 | 141 | **69** |

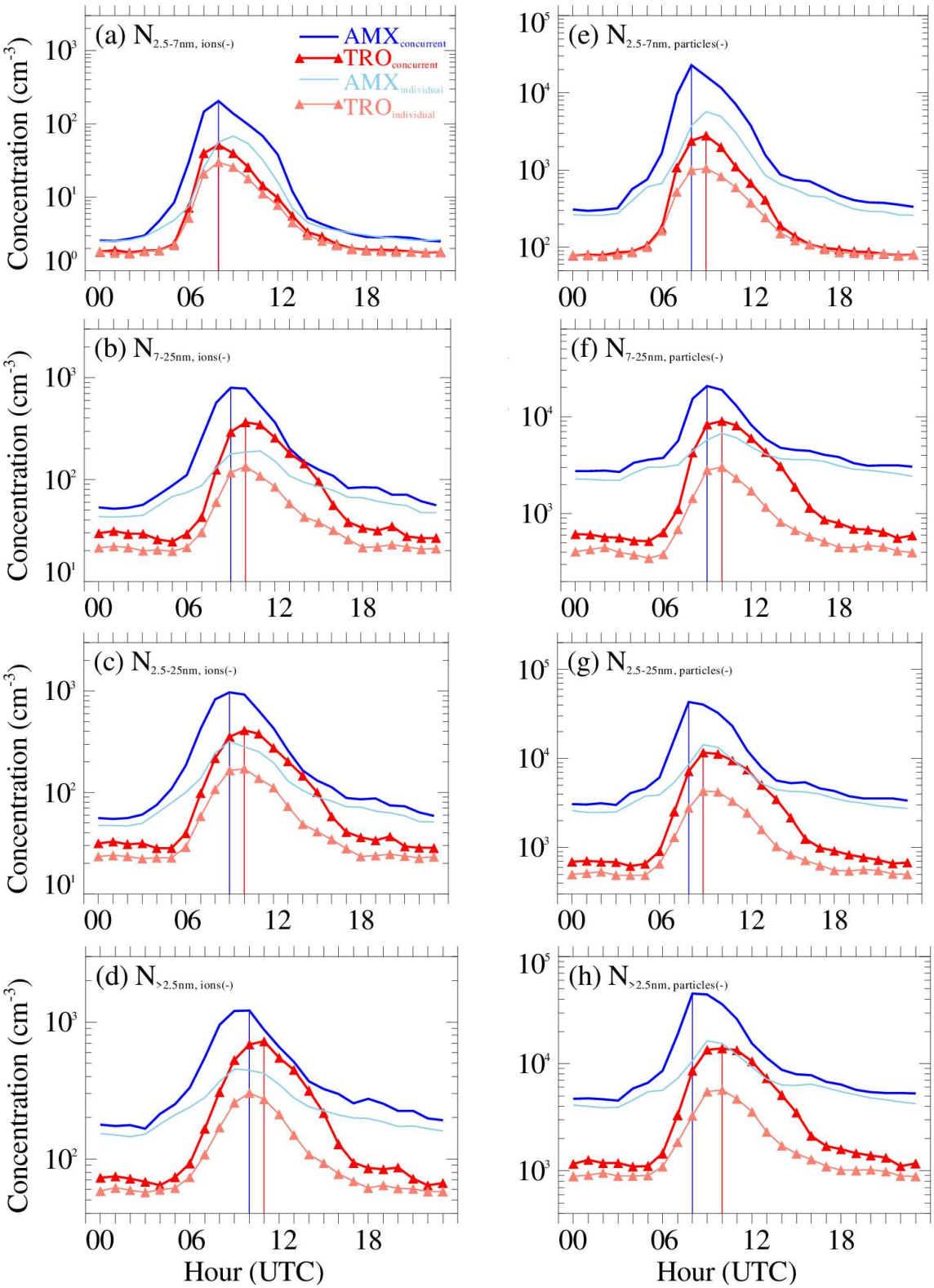


**Figure S2.** Median diurnal variation of negative polarity ion (a-d) and particle (e-h) size-segregated (2.5-7 nm, 7-25 nm, 2.5-25 nm, and >2.5 nm) number concentrations observed on concurrent NPF events at AMX (dark blue thick line) and TRO (dark red thick line). The light blue and light red coloured thin lines are for NPF events observed individually at AMX and TRO, respectively. The blue and red vertical lines indicate the times at which the peak concentrations for concurrent NPF events are observed at AMX and TRO, respectively.

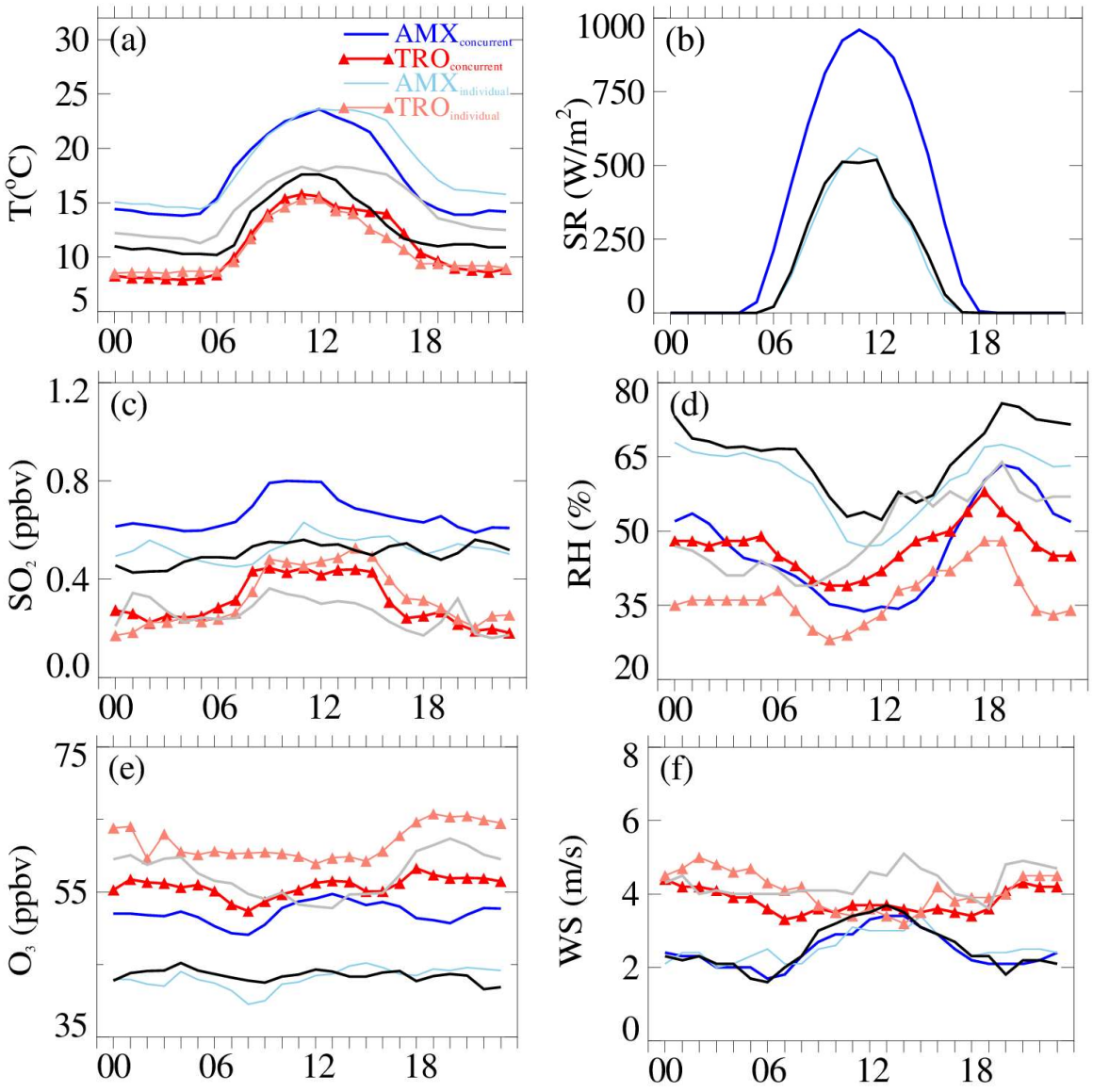


**Figure S3.** Median diurnal variation of in-situ measured meteorological parameters, such as (a) air temperature (T), (b) solar radiation (SR), (c) sulfur dioxide ($SO_2$), (d) relative humidity (RH), (e) ozone ($O_3$), and (f) wind speed (WS) for the observed concurrent NPF events at AMX (blue thick line) and TRO (red thick line). The light blue and light red coloured thin lines are for NPF events observed individually at AMX and TRO, respectively. Black and grey lines are for non-events observed at AMX and TRO, respectively.

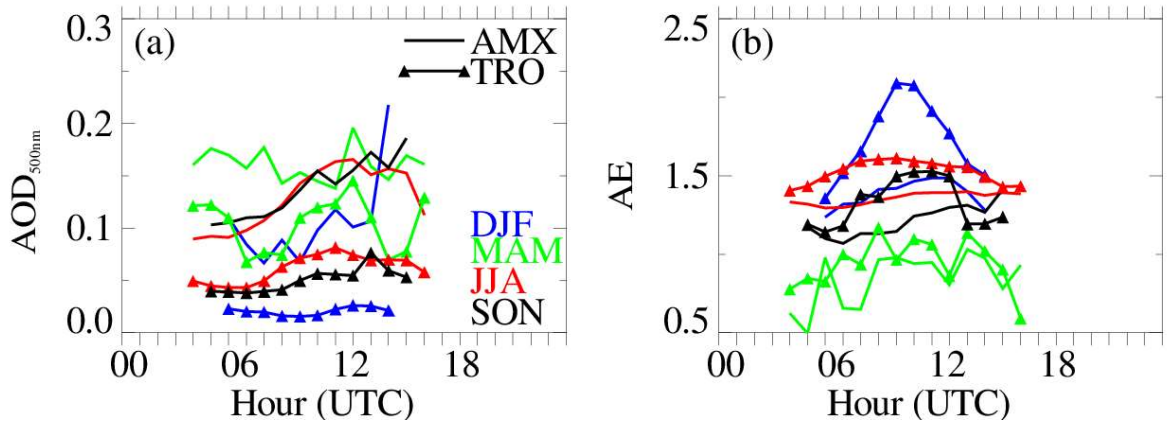


**Figure S4.** Median seasonal diurnal variation of AERONET derived (a) aerosol optical depth (AOD) and (b) Ångstrom exponent (AE) for winter (blue), spring (green), summer (red), and fall (black) based on the entire study period viz., from 1 January to 31 December 2022 at AMX (solid line) and TRO (line connected by filled triangles).

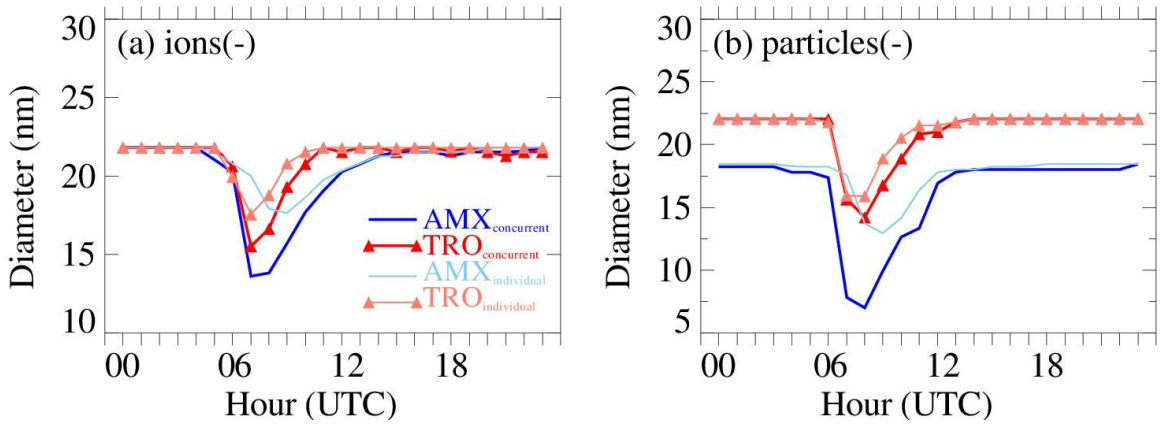


**Figure S5.** Median diurnal variation of negative polarity (a) ion and (b) particle mode diameter for the observed concurrent NPF events at AMX (blue thick line) and TRO (red thick line). The light blue and light red coloured thin lines are for NPF events observed individually at AMX and TRO, respectively.

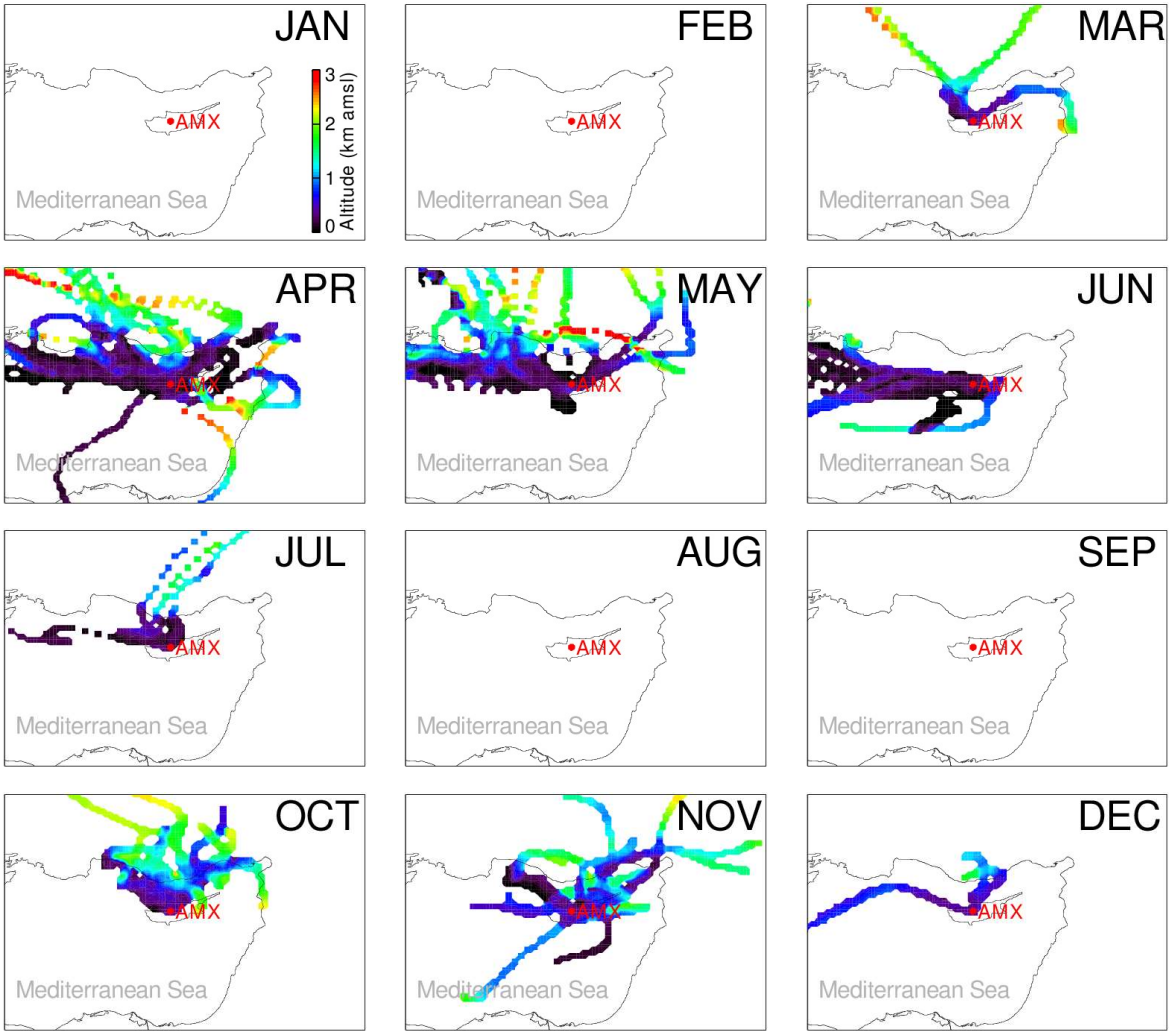


**Figure S6.** Monthly averaged two-day airmass backward trajectories as a function of altitude for observed concurrent NPF events at the AMX site.

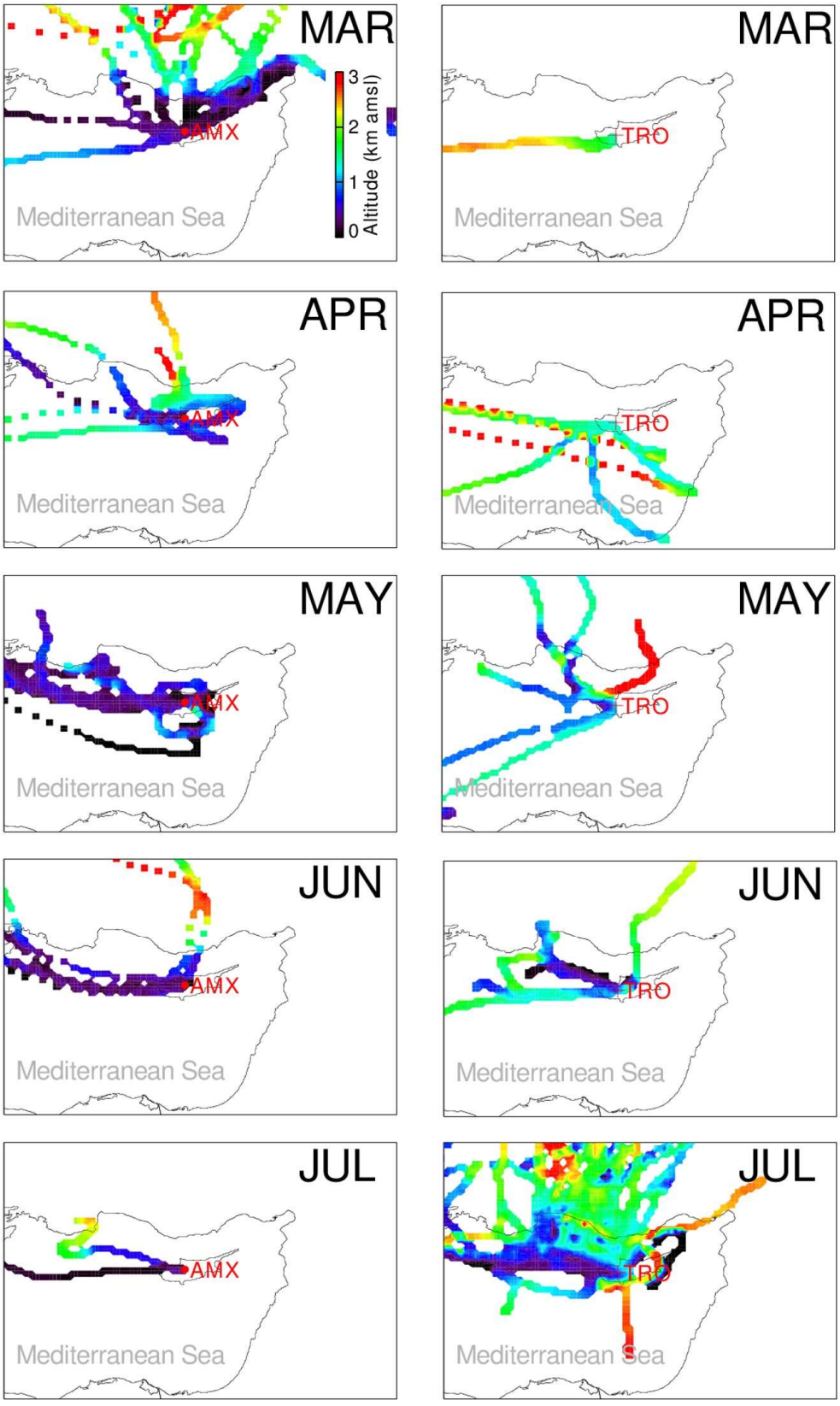


**Figure S7.** Same as Fig. S6, but for observed individual NPF events at AMX (left column) and TRO (right column). There were no measurements at AMX during August and September and at TRO during January, February, and December. All the observed NPF events during October and November concurrently occurred at both sites.